

Earlier Onset of Tumoral Angiogenesis in Matrix Metalloproteinase-19–Deficient Mice

Maud Jost,¹ Alicia R. Folgueras,³ Françoise Frérart,¹ Alberto M. Pendas,^{3,4} Silvia Blacher,¹ Xavier Houard,¹ Sarah Berndt,¹ Carine Munaut,¹ Didier Cataldo,¹ Jesus Alvarez,³ Laurence Melen-Lamalle,¹ Jean-Michel Foidart,^{1,2} Carlos López-Otín,³ and Agnès Noël¹

¹Laboratory of Tumor and Developmental Biology, Center for Experimental Cancer Research, Center for Biomedical Integrative Genoproteomics, University of Liège, Tour de Pathologie (B23); ²Department of Gynecology, Centre Hospitalier Universitaire, Liège, Belgium; ³Departamento de Bioquímica y Biología Molecular, Facultad de Medicina, Instituto Universitario de Oncología, Universidad de Oviedo, Oviedo, Spain; and ⁴Centro Investigacion Cancer, Salamanca, Spain

Abstract

Among matrix metalloproteinases (MMP), MMP-19 displays unique structural features and tissue distribution. In contrast to most MMPs, MMP-19 is expressed in normal human epidermis and down-regulated during malignant transformation and dedifferentiation. The contribution of MMP-19 during tumor angiogenesis is presently unknown. In an attempt to give new insights into MMP-19 *in vivo* functions, angiogenic response of mutant mice lacking MMP-19 was analyzed after transplantation of murine malignant PDVA keratinocytes and after injection of Matrigel supplemented with basic fibroblast growth factor. *In situ* hybridization and immunohistochemical analysis revealed that MMP-19 is produced by host mesenchymal cells but not by endothelial capillary cells or CD11b-positive inflammatory cells. Based on a new computer-assisted method of quantification, we provide evidence that host MMP-19 deficiency was associated with an increased early angiogenic response. In addition, increased tumor invasion was observed in MMP-19^{-/-} mice. We conclude that, in contrast to most MMPs that promote tumor progression, MMP-19 is a negative regulator of early steps of tumor angiogenesis and invasion. These data highlight the requirement to understand the individual functions of each MMP to improve anticancer strategies. (Cancer Res 2006; 66(10): 5234-41)

Introduction

Matrix metalloproteinases (MMP) are a family of structurally related zinc-dependent neutral endopeptidases that play major roles in tissue remodeling occurring in a variety of physiologic processes, such as embryonic development, angiogenesis, and wound healing (1, 2). They are main effectors of pathologic extracellular matrix destruction in many diseases, such as arthritis, atherosclerosis, age-related macular degeneration, tumor invasion, and metastasis (3–7). MMPs contribute to the fine tuning of diverse biological processes through limited proteolysis of specific targets, including not only matrix components, but also growth factors, chemokines/cytokines, and cell surface receptors (8–11). More than 20 different human MMPs have been identified (12) and classified

into different subfamilies according to their primary structure, domain organization, cellular localization, and substrate specificity (11, 13, 14). Produced as latent forms, they are either secreted in the extracellular medium or associated to the cell membrane (membrane-type MMPs; refs. 7, 11, 14).

Among MMPs, MMP-19 displays unique structural features and tissue distribution. Human MMP-19 cDNA was initially cloned from liver and mammary gland and was also identified as an autoantigen in inflamed rheumatoid synovium (15, 16). MMP-19 presents the typical domain organization of soluble MMPs, including a signal sequence, a propeptide maintaining enzyme latency, a catalytic domain with the typical zinc-binding motif, a linker region, and a COOH-terminal fragment with sequence similarity to hemopexin (15). However, MMP-19 displays several structural features distinctive of the diverse MMP subfamilies, including (a) an unique insertion of glutamic acid residues within the linker region, (b) an unusual latency motif in propeptide domain, (c) an additional cysteine residue in catalytic region, and (d) a COOH-terminal extension lacking sequence similarity to equivalent regions in other human MMPs (15, 17, 18). The catalytic domain of MMP-19 is capable of degrading components of basement membrane (laminin, type IV collagen, nidogen), connective tissue (fibronectin, type I gelatin), and cartilage (cartilage oligomeric matrix protein and aggrecan), but does not degrade triple-helical type I collagen (19, 20). In contrast to most other MMPs, MMP-19 is expressed in human mammary or skin epithelial cells under normal quiescent conditions and down-regulated in invasive carcinomas (21–23).

Evidence for MMP-19 involvement in tissue remodeling events, such as those occurring during adipogenesis and tumor progression, have been provided by the recent generation of MMP-19-deficient mice (24). Although lack of MMP-19 did not affect mice viability, fertility, and development, it led to a diet-induced obesity and a decreased susceptibility to skin tumors induced by chemical carcinogens. A role of MMP-19 during angiogenesis is suggested by its expression in endothelial cells of synovial capillaries following injury and inflammation (3, 25). However, the *ex vivo* sprouting of endothelial cells from aortic rings was not affected by MMP-19 deficiency (24). Therefore, the contribution of MMP-19 during angiogenic processes remains controversial. To give new insights into MMP-19 functions *in vivo*, the angiogenic response of mutant mice lacking MMP-19 was analyzed after transplantation of malignant murine PDVA keratinocytes and after injection of Matrigel supplemented with basic fibroblast growth factor (bFGF). In contrast to other single or double MMP-deficient mice studied until now, MMP-19-deficient mice exhibited an early onset of angiogenesis and tumor invasion.

Note: D. Cataldo is a scientific research worker from the Fonds National de la Recherche Scientifique (Belgium).

Requests for reprints: Agnès Noël, Laboratory of Tumor and Developmental Biology, University of Liège, Tour de Pathologie (B23), Sart-Tilman, B-4000 Liège, Belgium. Phone: 32-4-366-25-69; Fax: 32-4-366-29-36; E-mail: agnes.noel@ulg.ac.be.

©2006 American Association for Cancer Research.
doi:10.1158/0008-5472.CAN-05-4315

Materials and Methods

MMP-19-null mice. Mice genetically deficient in MMP-19 (*MMP-19*^{-/-}) were generated by replacing a portion of 1 kb of the promoter and exons 1 and 2 of the gene with a phosphoglycerate kinase-neomycin fusion gene and by homologous recombination (24). Homozygous *MMP-19*^{-/-} mice and their corresponding wild type (WT; *MMP-19*^{+/+}) were littermates deriving from interbreeding of heterozygotes with a mixed background of C57Bl6/1290la. When applying the transplantation chamber assay to mice with different genetic background, we previously showed that the extent of tumor invasion and vascularization was similar in all WT mice, independently to the number of backcrosses in C57Bl6 mice (26). Mice experimentation was done in accordance to guidelines of the University of Liège regarding the care and use of laboratory animals.

Transplantation assay in mice. PDVA cells were generated by *in vitro* carcinogen treatment (dimethylarsinic acid) of cultured keratinocytes issued from B10LP mice (27). PDVA cells were grown in modified Eagle's MEM containing a 4-fold concentration of amino acids and vitamins (Life Technologies Laboratories, Grant Island, NY), 10% FCS (Life Technologies), and antibiotics in a humidified incubator at 37°C, 5% CO₂. Cells (2 × 10⁵) were seeded on a collagen gel (4 mg/mL of type I collagen isolated from rat tail tendons) inserted in Teflon rings (Renner GmbH, Darmstadt, Germany). After 24 hours of culture, cell-coated collagen gels were covered with a silicone transplantation chamber (Renner) and implanted *in toto* onto dorsal muscle fascia of 6 to 8 weeks old mice according to the procedure previously described (28, 29). At different time points, tumor transplants were resected, embedded in Tissue Tek (Miles Laboratories, Inc., Naperville, IL), and frozen in liquid nitrogen for cryostat sectioning. Two hours before sacrifice, mice were *i.p.* injected with 200 µL BrdUrd/BrdC (65 µmol/L, Acros Organics, Geel, Belgium). Each experimental group contained at least six animals. Tumor angiogenesis and invasion in *MMP-19*^{-/-} and WT mice were evaluated in three independent sets of experiment.

Histologic analysis. Cryostat sections were fixed in acetone at -20°C and in 80% methanol at 4°C. For immunofluorescence labeling, the following antibodies were used: anti-type IV collagen antibody (rabbit polyclonal antibody; diluted 1/100), antikeratin antibody (polyclonal guinea pig antibody; diluted 1/20, Sigma-Aldrich, St. Louis, MO), anti-BrdUrd-FITC (monoclonal mouse, diluted 1/3.5, Becton Dickinson, San Diego, CA), anti-hinge region of MMP-19 (rabbit anti-human, diluted 1/20, Sigma-Aldrich; rabbit anti-human, diluted 1/500, Abcam, Cambridge, MA), anti-MMP-19 prodomain (rabbit anti-human, diluted 1/500, Abcam), anti-CD11b/tetramethyl-rhodamine isothiocyanate (TRITC; rat anti-mouse, diluted 1/50, PharMingen, San Diego, CA), anti- α -smooth muscle actin (α -SMA)/FITC (monoclonal mouse antibody, diluted 1/200, Sigma-Aldrich). When double-immunofluorescence labelings were done, after an incubation for 1 hour with primary antibodies, sections were washed with PBS and then incubated for 30 minutes with FITC- or TRITC-conjugated appropriate secondary antibodies: swine anti-rabbit (diluted 1/40, DAKO, Glostrup, Denmark), mouse anti-guinea pig (diluted 1/40, Sigma-Aldrich), or goat anti-rat (diluted 1/100, Molecular Probes, Carlsbad, CA). After three washes in PBS, coverslips were mounted with Aqua Polymount (Polysciences, Warrington, FL) and specific labeling was observed using an inverted microscope equipped with epifluorescence optics. Sections were counterstained in blue with bisbenzimidazole. At all times after grafting, collagen type IV labelings were codistributed with endothelial cells recognized by the anti-mouse PECAM immunostaining (data not shown).

Apoptosis was studied by terminal deoxynucleotidyl transferase-mediated dUTP nick-end labeling (TUNEL). Cryostat sections fixed in 4% paraformaldehyde for 20 minutes and in methanol for 5 minutes were stained for apoptosis following instructions of the manufacturer (Roche Diagnostics, Mannheim, Germany).

For quantitative measurement of proliferating cells, automatic computer-assisted image analysis was done on images obtained after bisbenzimidazole staining and immunolabeling of BrdUrd-positive cells. The ratio between the surface of bisbenzimidazole staining and the surface of specific immunostaining was measured by using a software Aphelion 3.2 from Adsis (Herouville Saint Clair, France).

In situ hybridization. Either sense or antisense ³⁵S-UTP-labeled RNA probes were synthesized from linearized cDNA fragment (1,600 bp) of mouse *MMP-19* gene cloned into *EcoRV* site of pcDNA3. Cryostat sections were hybridized with ³⁵S-labeled MMP-19 riboprobes and then exposed to photographic emulsion at 4°C for 6 days. Sections were developed, fixed, cleared, and counterstained with 0.02% toluidine blue. Bright field and dark field images were captured with a SPOT digital camera.

Scoring of tumor invasion and vascularization. For semiquantitative analysis of tumor vascularization, the following scoring was used: +, vessels below the collagen gel or infiltrating the collagen gel without reaching the malignant epithelial layer; ++, blood vessels in close apposition to the epithelial layer; and +++, blood vessels intermingled with invasive epithelial tumor sprouts (29).

Morphometric measurements of tumor cell invasion (average distance of invasion) and tumor vascularization (endothelial cell migration) were done by using a computer-assisted image analysis system (Olympus Micro Image version 3.0 for Windows 95/NT, Olympus Optical Co., Europe GmbH, Tokyo, Japan; ref. 30). Angiogenesis was quantified by measuring the distance (*d*) separating tumor cells from the front of migrating blood vessels. Therefore, the distance *d* is inversely related to the degree of endothelial cell migration. At least five measurements of distance (*d*) were done in the central part of each tumor and the mean values are reported.

Quantitative measurement of tumor invasion and angiogenesis by computer-assisted image processing. For quantitative measurements, automatic computer-assisted image analysis was done on images obtained after double immunostainings of keratinocytes (in green) and vessels (in red). The software Aphelion 3.2 from Adsis was used on a personal computer. Images were first digitized in 760 × 570 pixels with 256 Gray levels. Tumor and vessel images were processed separately. For tumor images, histogram equalization was first done to optimize the contrast. Then, tumor images were binarized/segmented automatically using the entropy of the histogram of the gray level intensities (31). For vessel images, vessels were binarized/segmented using an automatic threshold transformation that maximizes the global average contrast of edges (32). The upper boundary of the tumor was then automatically detected using a hit or miss transformation with an appropriate neighborhood configuration. A grid was constructed with the successive dilations (*n* = 1, 2, 3...) of this upper boundary, with a vertical line as structuring element. Tumor and vessel densities were determined on each interval of the grid, and the results drawn in function of the distance to the upper limit of the tumor. The largest distance of tumor invasion gives the thickness of the tumor. Quantification was done on each mouse in all independent assays. To compare the different distributions, the ANOVA was done and results were considered significantly different when the *P* value was <0.05.

Matrigel plug assay. A total of 0.5 mL Matrigel (10 mg/mL) mixed with 250 ng bFGF (R&D Systems, Minneapolis, MN) and 20 units heparin (Leo Pharma, Ballerup, Denmark; ref. 33) was *s.c.* injected in the abdominal midline region of 8-week-old *MMP-19* null and WT mice. After 7 days, animals were euthanized and Matrigel implants were harvested, frozen on dry ice, and lyophilized overnight. Dry plugs were weighed and suspended in 0.4 mL of 0.1% saponin (Calbiochem, La Jolla, CA) for 1 hour at 4°C, disrupted by vigorous pipetting and centrifuged at 15,000 × *g* for 15 minutes, at 4°C to remove particulates. Concentration of hemoglobin in the supernatant was determined after dilution in Drapkin's solution by measuring the absorbance at 560 nm (Drapkin reagent kit 525, Sigma, St. Louis, MO). A standard curve was done by using purified hemoglobin (Sigma). The angiogenic index corresponds to µg of hemoglobin per mg of Matrigel.

Statistical analysis. All experimental data are reported as mean ± SE, and statistical analysis was done by χ^2 test or Mann-Whitney test. *P* < 0.05 was considered as significant.

Results

Lack of MMP-19 increased the onset of skin tumor vascularization. Malignant PDVA keratinocytes cultured on a collagen gel were implanted onto the dorsal muscle fascia of *MMP-19*^{-/-} and *MMP-19*^{+/+} mice. To compare evolution of tumor

invasion and vascularization in these genotypes, transplants were resected after 14 and 21 days and angiogenesis was visualized after staining for collagen type IV to delineate capillary basement membranes (Fig. 1). Tumor grafting led to a remodeling of collagen matrix and a progressive infiltration by host-derived cells, including endothelial cells and inflammatory cells. Tumor vascularization was semiquantitatively scored according to the progressive migration of blood vessels toward tumor cells (Fig. 1). At day 14, in *MMP-19+/+* mice, blood vessels remained below the collagen gel or started to infiltrate it and all samples were scored + (Fig. 1A).

Tumor vascularization in *MMP-19-/-* mice was increased because 63% and 37% of transplants were scored + and ++, respectively ($P < 0.05$, χ^2 test; Fig. 1B). At that time, in both genotypes, tumor layer appeared as an irregular stratified epithelium on top of the collagen gel (Fig. 1A).

Vascularization of tumor transplants at day 14 was first quantified by measuring the distance (d) separating the bottom of tumor layer from the front of migrating blood vessels (Fig. 1D). This variable is inversely related to the degree of endothelial cell migration. Compared with *MMP-19+/+* mice, vessels migrated over

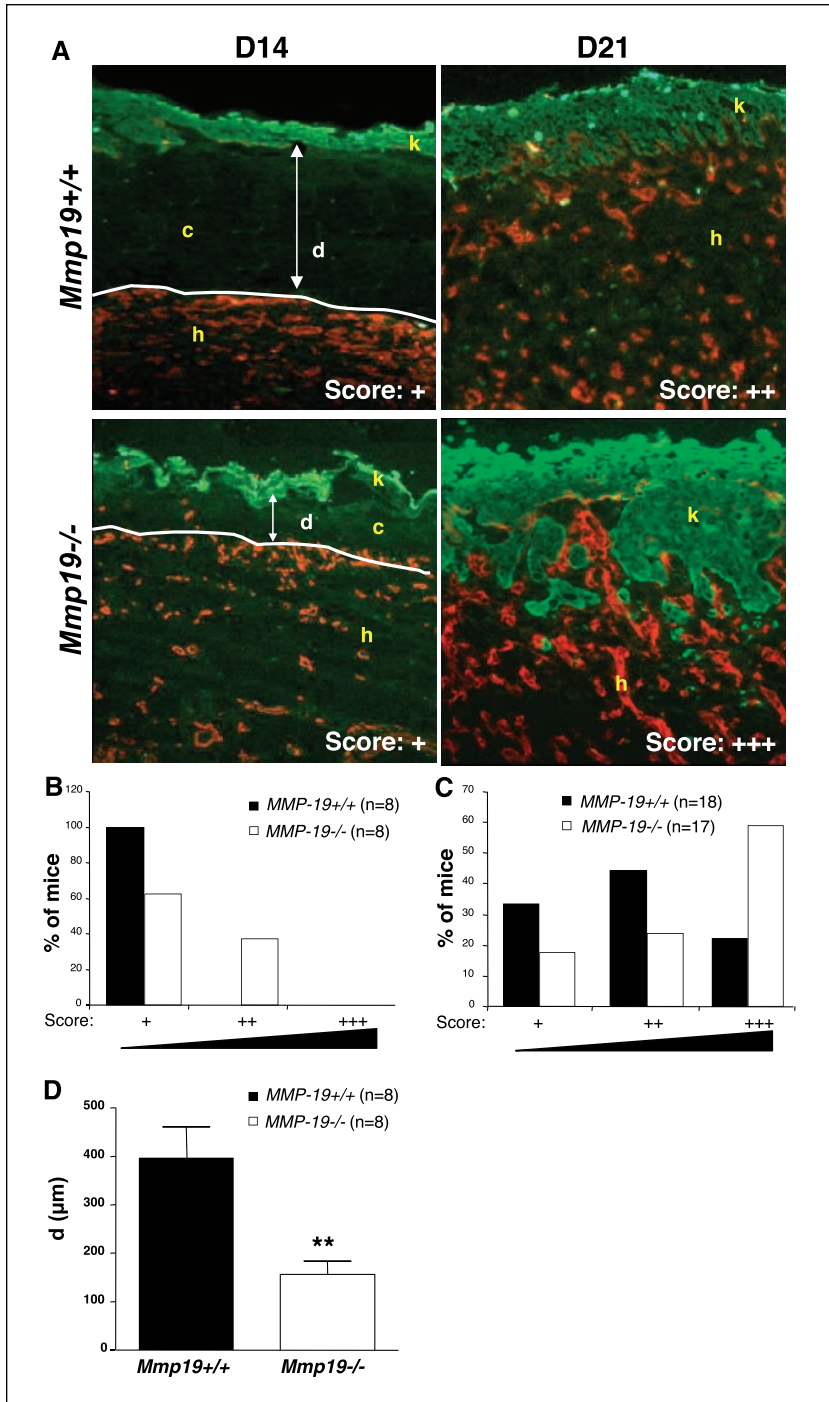


Figure 1. A, histologic analysis of tumor transplants. Immunofluorescence labeling of malignant keratinocytes and vessels in tumors transplanted into *MMP-19+/+* or *MMP-19-/-* mice observed after 14 days (D14) or 21 days (D21). Malignant cells (green, antikeratin antibody) and vessels (red, anticollagen type IV antibody) are visualized. Dotted line, front of endothelial cell migration. Scores and morphometric variable (d) used to quantify tumor invasion and angiogenesis are indicated (original magnification, $\times 200$). B to C, semiquantitative evaluation of tumor vascularization in *MMP-19+/+* (black columns) or *MMP-19-/-* mice (white columns). Tumors were scored as shown in A and in Materials and Methods. n , number of animals per group. D, quantification of tumor vascularization in tumors transplanted for 14 days in *MMP-19+/+* (black columns) or *MMP-19-/-* (white columns) mice. d , distance separating tumor cell layer from the front of migrating blood vessels as defined in A (see Materials and Methods; **, $P \leq 0.01$, Mann-Whitney test; $n = 8$). k , malignant keratinocytes; c , collagen gel; h , host tissue.

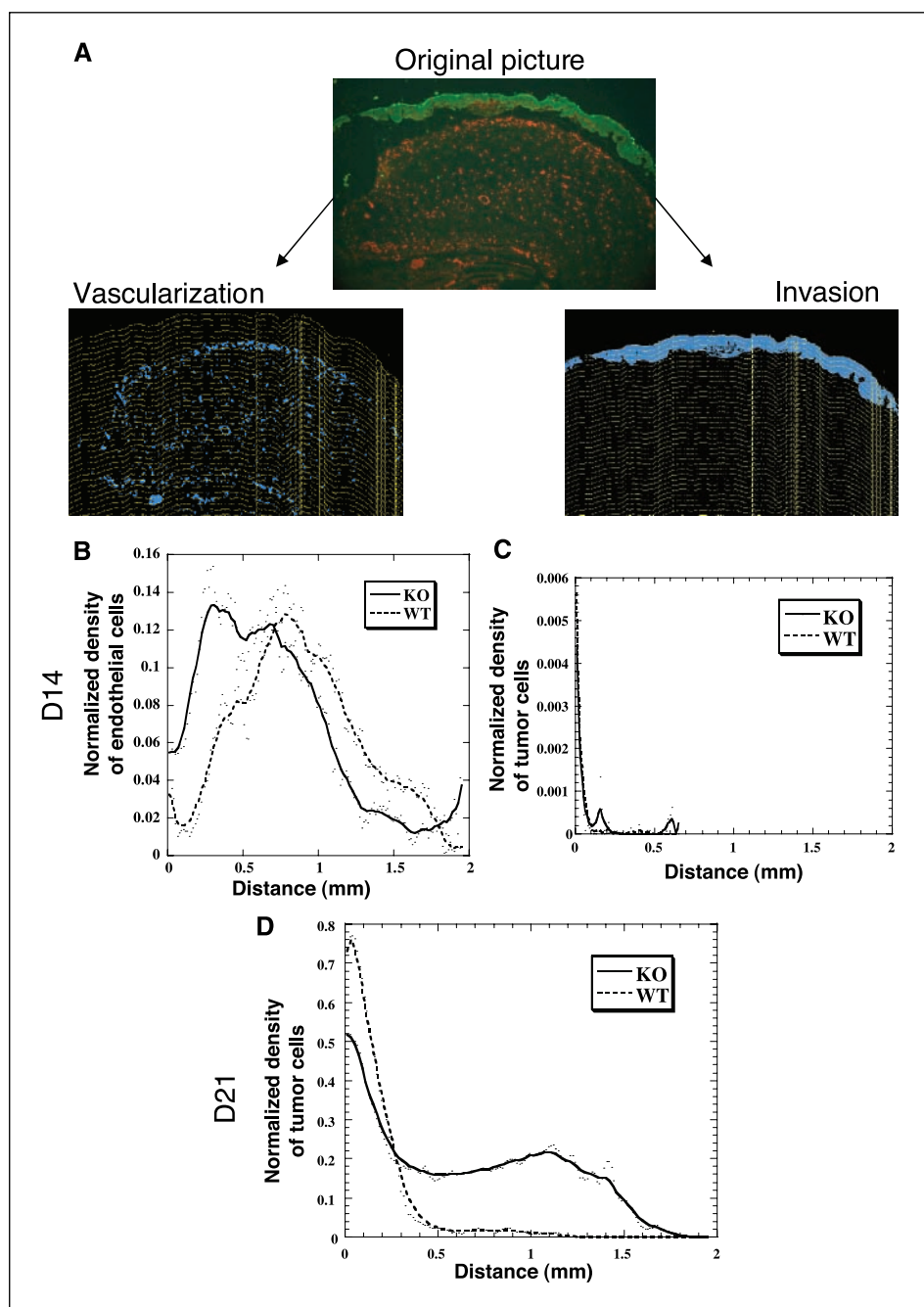


Figure 2. Quantification of tumor vascularization and invasion in tumor transplants based on computer-assisted image analysis. *A*, image processing of a typical transplant section. Malignant keratinocytes (green) and vessels (red; original image) were immunostained according to the procedure described in Materials and Methods. Images are binarized with extraction of vessels (Vascularization) or of tumor cells (Invasion). Tumor vascularization and tumor invasion were determined by using a grid obtained by successive dilation of the tumor upper border. *B* to *D*, determination of vessel density (normalized density of endothelial cells; *B*) and tumor cell density (normalized density of tumor cells; *C* and *D*) as a function of the distance to the upper boundary of tumor layer. The maximal distance of tumor cell invasion corresponds to tumor thickness (*D*). Malignant keratinocytes were transplanted into *MMP-19*^{+/+} (WT) and *MMP-19*^{-/-} (KO) mice for 14 or 21 days.

a higher distance in *MMP-19*-deficient mice (Fig. 1*D*). Indeed, the distance separating endothelial cells to malignant keratinocytes was 2.5-fold reduced in *MMP-19* null mice than in their corresponding WT littermates ($P = 0.0062$, Mann-Whitney test; Fig. 1*D*).

The observed increased blood vessel migration in *MMP-19*-null mice prompted us to set up a more objective quantitative method to investigate the spatial distribution of blood vessels in the remodeled matrix. With this aim, an original method based on computer-assisted image analysis was developed (Fig. 2*A*). The density of vessels picked already at a distance of around 0.25 mm from the upper boundary of tumor layer in *MMP-19*^{-/-} mice (Fig. 2*B*). In sharp contrast, the maximal density of endothelial cells

was observed at a distance of around 0.75 mm in *MMP-19*^{+/+} mice. A computer-assisted method of image analysis was also set up to quantify tumor cell invasion (Fig. 2*A*). At day 14 time point, no invasion was observed (Fig. 2*C*). This was expected because in the transplantation chamber assay, infiltration of vessels through the collagen gel toward tumor cells always precedes recognizable tumor cell invasion (34). Therefore, at early time point, *MMP-19*-deficient mice exhibited an acceleration of blood vessel infiltration in the remodeled matrix.

Lack of *MMP-19* increased tumor invasion. At day 21, once blood vessels have reached tumor cell layers, malignant keratinocytes formed tumor sprouts that invaded downward the remodeled host tissue and were intermingled with closely apposed new vessels

(Fig. 1A). Such vascularization pattern scored +++ was observed in ~60% (10 of 17) of *MMP-19*^{-/-} mice and only 22% (4 of 18) of *MMP-19*^{+/+} mice ($P = 0.027$, χ^2 test; Fig. 1C).

At this time point, the distance (d) separating tumor layer from the front of recruited blood vessels (Fig. 1) cannot be measured because in >70% of tumor transplants, vessels have reached the tumor layer (tumors scored ++ or +++). Therefore, for quantitative assessment, our original method of image analysis (Fig. 2) was applied to determine the malignant keratinocyte density as a function of the distance to the top of tumor transplant (Fig. 2D). In WT mice, keratinocyte density decreased abruptly with the distance to the top of tumor layer (Fig. 2D). Only few keratinocytes were observed at a distance >0.5 mm from the top of tumor layer. In sharp contrast, in *MMP-19* null mice, tumor cell density decreased more slowly and numerous malignant keratinocytes migrated over a distance of 0.5 mm. The maximal distance of keratinocyte migration was 1.2 and 1.8 mm in *MMP-19*^{+/+} and *MMP-19*^{-/-} mice, respectively (Fig. 2D). Therefore, a significant increase of tumor invasion was observed in the absence of host *MMP-19*.

This tumor-promoting effect observed in absence of *MMP-19* was not related to a modification of tumor cell proliferation rate as assessed by BrdUrd incorporation. Indeed, quantitative assessment done by computer-assisted image analysis revealed that the percentage of proliferating cells was similar in both genotypes 14 and 21 days after tumor transplantation (Fig. 3). Furthermore, TUNEL stainings for apoptotic cells indicated that the extent of apoptosis was identical and always low in cancer cell layers as well as in stromal strands of transplants resected from WT mice and *MMP-19*^{-/-} mice (data not shown).

***MMP-19* is produced by host stromal cells.** As a first step in determining the cellular source of *MMP-19*, *in situ* hybridization was done on tumors transplanted into *MMP-19*-proficient and *MMP-19*-deficient mice. Hybridization signals for *MMP-19* mRNAs were found in the stroma of WT mice (Fig. 4A) but not in that of knockout (KO) mice (Fig. 4C). No positive signal was detected after treatment with sense riboprobe used as negative controls (Fig. 4B). Immunohistochemical staining of tumor transplants confirmed the stromal production of *MMP-19* (Fig. 5A). This protease was produced by mesenchymal cells (Fig. 5A) but not by inflammatory cells positive for CD11b staining (Fig. 5C). Interestingly, *MMP-19* was not associated with capillaries newly formed in the remodeled collagen matrix (data not shown). In contrast, *MMP-19* staining was detected in large vascular structures present deeply in the host tissue, below tumor transplants (Fig. 5B). These vessels were positive for α -SMA and correspond to quiescent mature vessels.

Lack of *MMP-19* increased angiogenesis in Matrigel plug assay. To further investigate the effect of *MMP-19* deficiency on angiogenesis *in vivo* and to determine whether the angiogenic response was dependent on the matrix encountered by endothelial cells during their migration, the Matrigel plug assay was applied to mutant mice. Matrigel supplemented with bFGF was s.c. injected into the abdomen of WT and mutant mice ($n = 8$) and harvested after 7 days. Quantitative analysis of angiogenesis was done by measuring hemoglobin content in implants giving quantitative information on functional vessels. In accordance to results obtained in transplantation chamber assay, the angiogenic response in *MMP-19*-deficient mice was 6-fold increased compared with that detected in WT mice (Fig. 6; $P < 0.05$) and was therefore independent on the type of matrix used (type I collagen versus a reconstituted basement membrane).

Discussion

The analysis of cancer susceptibility in individual *MMP*-null mice is of growing interest after the failure of synthetic *MMP* inhibitors in clinical trials and the finding of multiple and even opposite roles of *MMPs* in tumor progression. We describe here that in contrast to most *MMP* deficiencies described up to now in mice, the angiogenic response was accelerated and tumor invasion was increased in *MMP-19*-deficient mice. This was evidenced by (a) an accelerated vascularization and a higher degree of tumor invasion after malignant keratinocyte transplantation and (b) an increased vascularization in bFGF-treated Matrigel implants in *MMP-19*^{-/-} mice.

The time course of malignant growth begins with an early onset of stromal activation and infiltration of inflammatory cells and endothelial cells. These key events can be mimicked in the transplantation system used here, which is a highly sensitive tool to inspect kinetics of early steps of host stromal response to tumor signals (34, 35). By applying this system to *MMP-19*^{-/-} mice, it seems that the angiogenic response was affected by lack of host *MMP-19*. Surprisingly, endothelial cell recruitment was significantly increased 14 days after transplantation, leading to an acceleration of tumor vascularization. Consequently, tumor invasion was increased in *MMP-19*-deficient mice 21 days after tumor transplantation. These findings indicate that *MMP-19* is a negative regulator of early steps of cancer angiogenesis and invasion.

By *in situ* hybridization and immunohistochemical analysis, we show that mesenchymal cells produce *MMP-19*, whereas

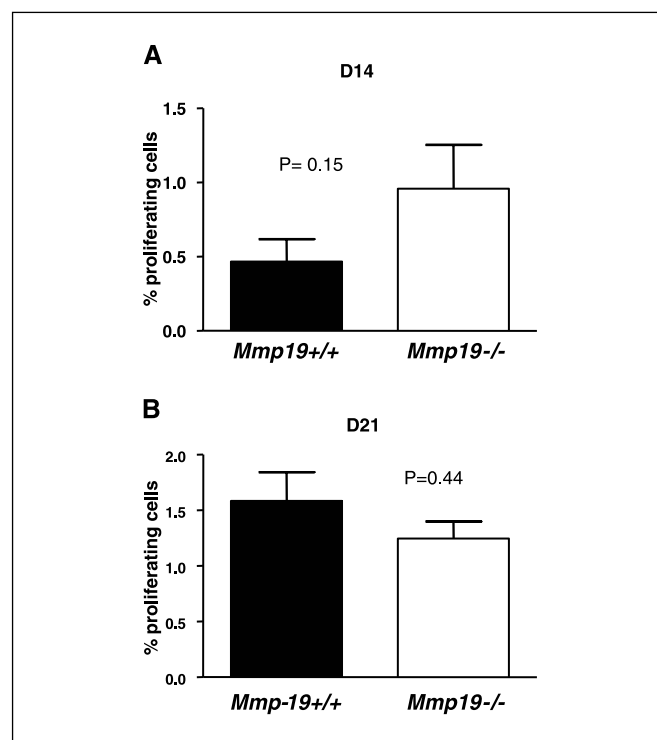


Figure 3. BrdUrd immunostaining of tumor transplants. Malignant keratinocytes were transplanted for 14 days (A) or 21 days (B) into *MMP-19*^{+/+} (black columns) or *MMP-19*^{-/-} (white columns) mice. Before sacrifice, mice were injected with BrdUrd and immunostaining was done on tumor sections. The percentage of positive cells was determined by a computer-assisted method described in Materials and Methods.

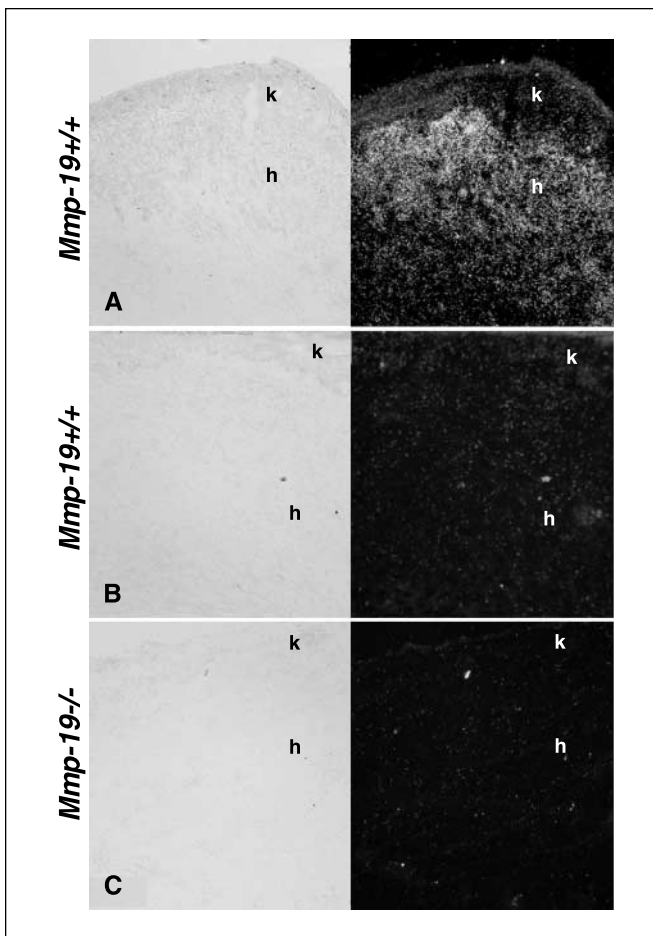


Figure 4. *In situ* hybridization of tumor transplants. Sections of malignant keratinocytes transplanted into *MMP-19*^{+/+} (A and B) and *MMP-19*^{-/-} (C) mice for 21 days were hybridized with ³⁵S-labeled antisense *MMP-19* riboprobe (A and C) or sense *MMP-19* riboprobe (B) used as negative control. Bright-field (left) and dark-field (right) images were both captured. Stromal cells in host tissue (h), but not malignant keratinocytes (k), were positively stained for *MMP-19* mRNAs (original magnification, $\times 100$).

CD11b-positive inflammatory cells and malignant keratinocytes do not express it. Accordingly, MMP-19 mRNA expression and pro-MMP-19 production by human fibroblasts have been detected *in vivo* in dermal wounds and in cultures of fibroblasts (36). In our model, MMP-19 is not produced by sprouting endothelial cells of neo-formed capillaries. This observation fits with our previous observation that MMP-19 is not required for *ex vivo* endothelial cell migration in a collagen gel in the aortic ring assay (24). According to the report of Kolb et al. (25), MMP-19 is associated with α -SMA-positive large vessels deeply embedded in the host tissue.

Taking into account its *in vitro* substrates (laminin-1, laminin-5, type IV collagen, fibronectin, tenascin-C, or nidogen), MMP-19 might play a key role in matrix degradation and tissue remodeling (19, 20, 37). A recent *in vitro* study suggests that through its capacity to cleave nidogen, MMP-19 could control formation of capillary structures on Matrigel by cultured endothelial cells (38). However, the *ex vivo* endothelial cell sprouting from mouse aortic rings in a three-dimensional matrix was not affected by *MMP-19* deficiency (24). Therefore, the accelerated angiogenic response observed *in vivo* in the

transplantation system could not be ascribed to a modified ability of endothelial cells to migrate or differentiate into capillary-like structures in a pure collagen matrix in the absence of MMP-19. Interestingly, the accelerated recruitment of endothelial cells *in vivo* was observed both in transplantation system using type I collagen and in Matrigel plug assay, suggesting that this effect of MMP-19 on angiogenesis was not dependent on the matrix used.

The identification of novel non-matrix substrates for MMPs has extended MMP functions beyond their classic role in extracellular matrix disruption (4, 11). The recent finding that MMP-19 cleaves *in vitro* insulin-like growth factor binding protein-3 (39) suggests that it could control the activity of insulin-like growth factors and thereby regulate cancer cell growth. However, in our system, tumor cell proliferation was not affected by MMP-19 deficiency. Similarly, tumor cell apoptosis was not modulated by the absence of host MMP-19. It is worth noting that proteolytic processing of some

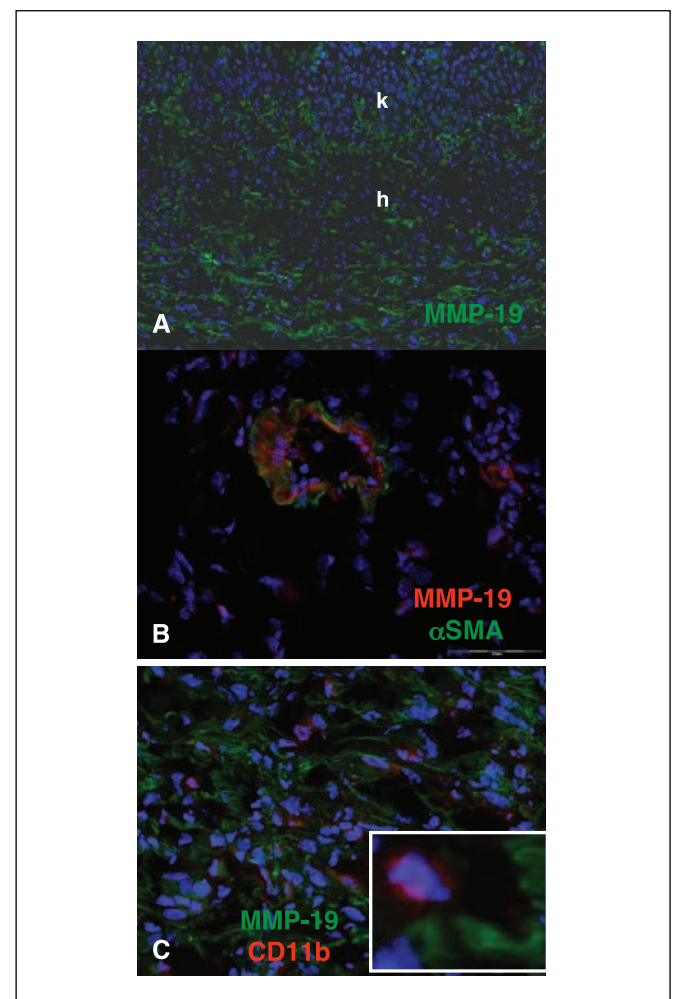


Figure 5. Immunostaining of tumors transplanted into WT mice. Sections are counterstained with bisbenzimidazole (blue staining). Host stromal cells are positive for MMP-19 immunostaining (green; original magnification, $\times 200$; A). Double immunostainings reveal that MMP-19 (red) is not present in newly formed vessels in collagen matrix but is associated to vascular structures stained with α -SMA antibody (green) and localized deeply in host tissue (original magnification, $\times 400$; B). MMP-19 (green) does not colocalize with CD11b-positive inflammatory cells (red; original magnification, $\times 400$; C). Higher magnification is shown in inset (C).

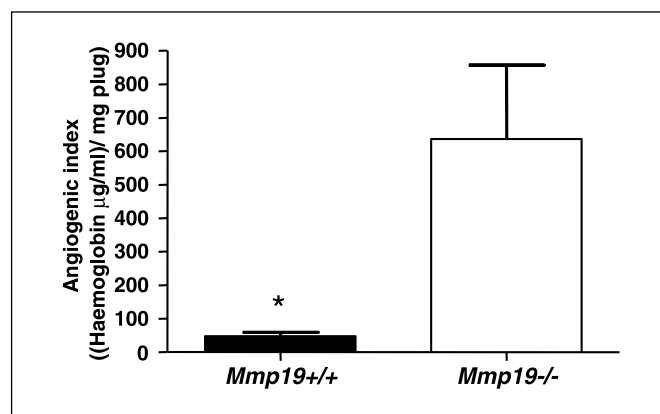


Figure 6. Increased vascularization in Matrigel plug containing bFGF and implanted in *MMP-19*^{-/-} mice. Functional vascularization was quantified by measuring hemoglobin concentration in Matrigel plug implanted into *MMP-19*^{+/+} and *MMP-19*^{-/-} mice. *, $P \leq 0.05$.

bioactive molecules, such as growth factors and/or cytokines/chemokines, could also indirectly contribute to microenvironment modifications promoting or inhibiting endothelial cell recruitment during angiogenesis onset. The assumption that MMPs are in general proangiogenic has been challenged by the finding that some of them could suppress neovascularization by generating angiogenic inhibitors (40). In this context, MMP-19 could exert its antiangiogenic effect through inactivation of angiogenic/chemotactic factors or production/maturation of angiogenic inhibitors. In addition, MMP-19 production in large quiescent host vessels present below tumor transplants, but not in growing capillaries, suggests a yet unknown functional role of this protease in maintenance of blood vessel stability. Its absence could destabilize endothelial cell-mural cell interactions, thereby initiating active sprouting events and endothelial cell migration. This hypothesis could explain the transient effect of MMP-19 deficiency at angiogenesis onset.

The present results do not negate the possibility that MMP-19 might have dual functions during cancer progression. In a model of methylcholanthrene-induced chemical carcinogenesis, we previously showed that *MMP-19*^{-/-} mice develop less fibrosarcomas and with a longer latency period than WT littermates (24). These apparently paradoxical results may reflect different roles of MMP-19 in the evolution of various cancer types (carcinoma versus fibrosarcoma), as well as throughout different steps of cancer progression. The down-regulation and disappearance of MMP-19 production observed during neoplastic progression in breast and skin carcinomas (21–23) are consistent with our data demonstrating a control of early steps of skin carcinoma

evolution by MMP-19. Altogether, these data based on clinical and experimental studies suggest that MMP-19 negatively regulates early stages of tumor cell invasion, but cancer cells could become less sensitive to MMP-19 activity once tumor develops. Temporal differences in effect of proteases on tumor growth and conversion to aggressive tumors have also been reported for MMP-9 (41) and MMP-11 (42).

By applying the same transplantation chamber assay into different single or double *MMP*-deficient mice (43), we previously reported that tumor invasion and angiogenesis were both impaired by the combined deficiency in *MMP-2* and *MMP-9* demonstrating that concomitant production of gelatinases is required for tumor invasion and vascularization. Therefore, although MMP-2 and MMP-9 are viewed as positive regulators of tumor angiogenesis (4, 41, 44, 45), MMP-19 could function in an opposite manner, slowing down the angiogenic process. These unexpected data are in accordance with the emerging antitumor properties of some MMPs. In this context, skin tumor susceptibility was increased in mice deficient for MMP-8 (46) or MMP-3 (47). Furthermore, our results support the view that MMPs act as sophisticated modulators rather than simple inducers or suppressors and highlight the functional complexity of MMP family during cancer progression. Some MMPs appear to have dual role in cancer progression by promoting angiogenesis and generating angiogenesis inhibitors (6). For instance, although MMP-7 and MMP-9 are both able to generate angiostatin (40), MMP-7 facilitates tumor progression in mouse models (48) and MMP-9 promotes tumor angiogenesis (41, 43–45). Increased expression of some MMPs may both confer increased tumor cell invasiveness and, paradoxically, lead to production of molecules that limit tumor growth. Altogether, these data point out the need to determine both spatial and temporal significance of individual MMP during cancer progression to design more rational MMP inhibitors.

Acknowledgments

Received 12/2/2005; revised 2/16/2006; accepted 3/14/2006.

Grant support: Communauté Française de Belgique (Actions de Recherches Concertées), the European Union (FP5 and FP6), the Fonds National de la Recherche Scientifique (Belgium), the Fédération Belge Contre le Cancer, the Centre Anticancéreux près l'Université de Liège, the FB Assurances, the Fondation Léon Frédéricq (University of Liège), the Direction Générale des Technologies, de la Recherche et de l'Énergie from the "Région Wallonne," the Interuniversity Attraction Poles Programme-Belgian Science Policy (Brussels, Belgium), the Comisión Interministerial de Ciencia y Tecnología (C. López-Otín), and Fonds National de la Recherche Scientifique-Télévie (M. Jost and S. Berndt).

The costs of publication of this article were defrayed in part by the payment of page charges. This article must therefore be hereby marked *advertisement* in accordance with 18 U.S.C. Section 1734 solely to indicate this fact.

We thank I. Dasoul, P. Gavittelli, F. Olivier, and G. Roland for their excellent technical assistance.

References

- Nagase H, Woessner JF. Matrix metalloproteinases. *J Biol Chem* 1999;274:21491–4.
- Vu TH, Werb Z. Matrix metalloproteinases: effectors of development and normal physiology. *Genes Dev* 2000; 14:2123–33.
- Kontinen YT, Ainola M, Valleala H, et al. Analysis of 16 different matrix metalloproteinases (MMP-1 to MMP-20) in the synovial membrane: different profiles in trauma and rheumatoid arthritis. *Ann Rheum Dis* 1999;58:691–7.
- Folgueras AR, Pendas AM, Sanchez LM, Lopez-Otin C. Matrix metalloproteinases in cancer: from new functions to improved inhibition strategies. *Int J Dev Biol* 2004;48:411–24.
- Noel A, Maillard C, Rocks N, et al. Membrane associated proteases and their inhibitors in tumour angiogenesis. *J Clin Pathol* 2004;57:577–84.
- Handsley MM, Edwards DR. Metalloproteinases and their inhibitors in tumor angiogenesis. *Int J Cancer* 2005; 115:849–60.
- Sounni NE, Noel A. Membrane type-matrix metalloproteinases and tumor progression. *Biochimie* 2005; 87:329–42.
- Sternlicht MD, Werb Z. How matrix metalloproteinases regulate cell behavior. *Annu Rev Cell Dev Biol* 2001;17:463–516.
- McQuibban GA, Gong JH, Tam EM, McCulloch CAG, Clark-Lewis I, Overall CM. Inflammation dampened by gelatinase A cleavage of monocyte chemoattractant protein-3. *Science* 2000;289:1202–6.
- McQuibban GA, Butler GS, Gong JH, et al. Matrix metalloproteinase activity inactivates the CXC chemokine stromal cell-derived factor-1. *J Biol Chem* 2001;276: 43503–8.
- Egeblad M, Werb Z. New functions for the matrix

- metalloproteinases in cancer progression. *Nat Rev Cancer* 2002;2:161-74.
12. Puente XS, Lopez-Otin C. A genomic analysis of rat proteases and protease inhibitors. *Genome Res* 2004;14:609-22.
 13. Lopez-Otin C, Overall CM. Protease degradomics: a new challenge for proteomics. *Nat Rev Mol Cell Biol* 2002;3:509-19.
 14. Zucker S, Pei DQ, Cao J, Lopez-Otin C. Membrane type-matrix metalloproteinases (MT-MMP). *Cell Surface Proteases* 2003;54:1-74.
 15. Pendas AM, Knauper V, Puente XS, et al. Identification and characterization of a novel human matrix metalloproteinase with unique structural characteristics, chromosomal location, and tissue distribution. *J Biol Chem* 1997;272:4281-6.
 16. Sedlacek R, Mauch S, Kolb B, et al. Matrix metalloproteinase MMP-19 (RASI 1) is expressed on the surface of activated peripheral blood mononuclear cells and is detected as an autoantigen in rheumatoid arthritis. *Immunobiology* 1998;198:408-23.
 17. Yang MZ, Kurkinen M. Cloning and characterization of a novel matrix metalloproteinase (MMP), CMMP, from chicken embryo fibroblasts-CMMP, *Xenopus* XMMP, and human MMP19 have a conserved unique cysteine in the catalytic domain. *J Biol Chem* 1998;273:17893-900.
 18. Mueller MS, Mauch S, Sedlacek R. Structure of the human MMP-19 gene. *Gene* 2000;252:27-37.
 19. Stracke JO, Fosang AJ, Last K, et al. Matrix metalloproteinases 19 and 20 cleave aggrecan and cartilage oligomeric matrix protein (COMP). *FEBS Lett* 2000;478:52-6.
 20. Stracke JO, Hutton M, Stewart M, et al. Biochemical characterization of the catalytic domain of human matrix metalloproteinase 19—evidence for a role as a potent basement membrane degrading enzyme. *J Biol Chem* 2000;275:14809-16.
 21. Djonov V, Hogger K, Sedlacek R, Laissue J, Draeger A. MMP-19: cellular localization of a novel metalloproteinase within normal breast tissue and mammary gland tumours. *J Pathol* 2001;195:147-55.
 22. Impola U, Toriseva M, Suomela S, et al. Matrix metalloproteinase-19 is expressed by proliferating epithelium but disappears with neoplastic dedifferentiation. *Int J Cancer* 2003;103:709-16.
 23. Impola U, Jeskanen L, Ravanti L, et al. Expression of matrix metalloproteinase (MMP)-7 and MMP-13 and loss of MMP-19 and p16 are associated with malignant progression in chronic wounds. *Br J Dermatol* 2005;152:720-6.
 24. Pendas AM, Folgueras AR, Llano E, et al. Diet-induced obesity and reduced skin cancer susceptibility in matrix metalloproteinase 19-deficient mice. *Mol Cell Biol* 2004;24:5304-13.
 25. Kolb C, Mauch S, Krawinkel U, Sedlacek R. Matrix metalloproteinase-19 in capillary endothelial cells: expression in acutely, but not in chronically, inflamed synovium. *Exp Cell Res* 1999;250:122-30.
 26. Bajou K, Masson V, Gerard RD, et al. The plasminogen activator inhibitor PAI-1 controls *in vivo* tumor vascularization by interaction with proteases, not vitronectin: implications for antiangiogenic strategies. *J Cell Biol* 2001;152:777-84.
 27. Fusenig NE. Growth and differentiation characteristics of transformed keratinocytes from mouse and human skin *in vitro* and *in vivo*. In: Breitkreutz D, Dzarlieva RT, Boukamp P, Bohnert A, Tilgen W, editors. *J Invest Dermatol* 1983;81:168-75.
 28. Bajou K, Noel A, Gerard RD, et al. Absence of host plasminogen activator inhibitor 1 prevents cancer invasion and vascularization. *Nat Med* 1998;4:923-8.
 29. Bajou K, Masson V, Gerard RD, et al. The plasminogen activator inhibitor PAI-1 controls *in vivo* tumor vascularization by interaction with proteases, not vitronectin: implications for antiangiogenic strategies. *J Cell Biol* 2001;152:777-84.
 30. Bajou K, Maillard C, Jost M, et al. Host-derived plasminogen activator inhibitor-1 (PAI-1) concentration is critical for *in vivo* tumoral angiogenesis and growth. *Oncogene* 2004;23:6986-90.
 31. Kapur JN, Sahoo PK, Wong AKC. A new method for Gray-level picture thresholding using the entropy of the histogram. *Comput Vis Graph Image Process* 1985;29:273-85.
 32. Kohler R. A segmentation system based on thresholding. *Comput Graph Image Process* 1985;15:319-38.
 33. Passaniti A, Taylor RM, Pili R, et al. Methods in laboratory investigation—a simple, quantitative method for assessing angiogenesis and antiangiogenic agents using reconstituted basement-membrane, heparin, and fibroblast growth-factor. *Lab Invest* 1992;67:519-28.
 34. Mueller MM, Fusenig NE. Tumor-stroma interactions directing phenotype and progression of epithelial skin tumor cells. *Differentiation* 2002;70:486-97.
 35. Mueller MM, Fusenig NE. Friends or foes—bipolar effects of the tumour stroma in cancer. *Nat Rev Cancer* 2004;4:839-49.
 36. Hieta N, Impola U, Lopez-Otin C, Saarialho-Kere U, Kahari VM. Matrix metalloproteinase-19 expression in dermal wounds and by fibroblasts in culture. *J Invest Dermatol* 2003;121:997-1004.
 37. Sadowski T, Dietrich S, Koschinsky F, et al. Matrix metalloproteinase 19 processes the laminin 5 γ 2 chain and induces epithelial cell migration. *Cell Mol Life Sci* 2005;62:870-80.
 38. Titz B, Dietrich S, Sadowski T, Beck C, Petersen A, Sedlacek R. Activity of MMP-19 inhibits capillary-like formation due to processing of nidogen-1. *Cell Mol Life Sci* 2004;61:1826-33.
 39. Sadowski T, Dietrich S, Koschinsky F, Sedlacek R. Matrix metalloproteinase 19 regulates insulin-like growth factor-mediated proliferation, migration, and adhesion in human keratinocytes through proteolysis of insulin-like growth factor binding protein-3. *Mol Biol Cell* 2003;14:4569-80.
 40. Pozzi A, Moberg PE, Miles LA, Wagner S, Soloway P, Gardner HA. Elevated matrix metalloproteinase and angiostatin levels in integrin α 1 knockout mice cause reduced tumor vascularization. *Proc Natl Acad Sci U S A* 2000;97:2202-7.
 41. Coussens LM, Tinkle CL, Hanahan D, Werb Z. MMP-9 supplied by bone marrow-derived cells contributes to skin carcinogenesis. *Cell* 2000;103:481-90.
 42. Andarawewa KL, Boulay A, Masson W, et al. Dual stromelysin-3 function during natural mouse mammary tumor virus-ras tumor progression. *Cancer Res* 2003;63:5844-9.
 43. Masson V, de la Ballina LR, Munaut C, et al. Contribution of host MMP-2 and MMP-9 to promote tumor vascularization and invasion of malignant keratinocytes. *FASEB J* 2005;19:234-6.
 44. Bergers G, Brekken R, McMahon G, et al. Matrix metalloproteinase-9 triggers the angiogenic switch during carcinogenesis. *Nat Cell Biol* 2000;2:737-44.
 45. Chantraine CF, Shimada H, Jodele S, et al. Stromal matrix metalloproteinase-9 regulates the vascular architecture in neuroblastoma by promoting pericyte recruitment. *Cancer Res* 2004;64:1675-86.
 46. Balbin M, Fueyo A, Tester AM, et al. Loss of collagenase-2 confers increased skin tumor susceptibility to male mice. *Nat Genet* 2003;35:252-7.
 47. McCawley LJ, Crawford HC, King LE, Mudget J, Matrisian LM. A protective role for matrix metalloproteinase-3 in squamous cell carcinoma. *Cancer Res* 2004;64:6965-72.
 48. Rudolph-Owen LA, Chan R, Muller WJ, Matrisian LM. The matrix metalloproteinase matrilysin influences early-stage mammary tumorigenesis. *Cancer Res* 1998;58:5500-6.